SECURITY CLASSIFICATION OF THIS PAGE

REPORT DOCUMENTATION PAGE

FILE COPY

1. AD-A214 440

1b. RESTRICTIVE MARKINGS

3. DISTRIBUTION/AVAILABILITY OF REPORT

4 PERFORMING ORGANIZATION REPORT NUMBER(S)

5. MONITORING ORGANIZATION REPORT NUMBER(S)

6a NAME OF PERFORMING ORGANIZATION: State University of New York Stony Brook, NY 11794-3800

6b. OFFICE SYMBOL (If applicable)

7a. NAME OF MONITORING ORGANIZATION: same as 8a

6c. ADDRESS (City, State and ZIP Code): Dept. of Physics, SUNY, Stony Brook, NY 11794

7b. ADDRESS (City, State and ZIP Code): Same as 8b

8a. NAME OF FUNDING/SPONSORING ORGANIZATION: Office of Naval Research

8b. OFFICE SYMBOL (If applicable)

9. PROCUREMENT INSTRUMENT IDENTIFICATION NUMBER: N0001483K0585

8c. ADDRESS (City, State and ZIP Code): 800 N. Quincy Avenue, Arlington, VA 22217

10 SOURCE OF FUNDING NOS

PROGRAM ELEMENT NO.	PROJECT NO.	TASK NO.	WORK UNIT NO

11. TITLE (Include Security Classification): Laser Cooling of Neutral Atoms

12. PERSONAL AUTHOR(S): Harold Metcalf

13a TYPE OF REPORT	13b. TIME COVERED	14. DATE OF REPORT (Yr., Mo., Day)	15 PAGE COUNT
Final	FROM 7/22/83 TO 9/30/88	October 1989	23

16. SUPPLEMENTARY NOTATION

17. COSATI CODES		
FIELD	GROUP	SUB. GR.

18. SUBJECT TERMS (Continue on reverse if necessary and identify by block number): Laser Cooling, Optical Molasses

19. ABSTRACT (Continue on reverse if necessary and identify by block number)

DTIC ELECTE NOV 14 1989 S B D

20. DISTRIBUTION/AVAILABILITY OF ABSTRACT

UNCLASSIFIED/UNLIMITED ☐ SAME AS RPT. ☐ DTIC USERS ☐

21. ABSTRACT SECURITY CLASSIFICATION

22a NAME OF RESPONSIBLE INDIVIDUAL	22b TELEPHONE NUMBER (Include Area Code)	22c OFFICE SYMBOL
Harold Metcalf	516-632-8185	

DD FORM 1473, 83 APR EDITION OF 1 JAN 73 IS OBSOLETE.

SECURITY CLASSIFICATION OF THIS PAGE

DISTRIBUTION STATEMENT A
Approved for public release;
Distribution Unlimited

89 11 08 032

INTRODUCTION

One way to measure progress is by the publication record, and by that criterion we have had an excellent year. Because of the high level of activity in this field, the Optical Society of America has designated that a special issue of its journal be devoted to the topic of optical forces on atoms, and we have submitted three papers to that issue. Since the total volume of these manuscripts exceeds 80 pages, they are not appended to this proposal. Copies have been sent to the cognizant program officer at O.N.R. Dr. Peter Reynolds. In addition, there have been several abstracts, as well as other papers in press or published, and all of these are tabulated in Appendix A.

A. Collimation of a Rubidium Atomic Beam

1. Introduction. We have discovered a new cooling process that uses an applied magnetic field to mix differentially light shifted atomic ground state sublevels. It seems to be another form of the "polarization scrambling" molasses that was appropriate for our ultra-cold measurements on the three dimensional Na molasses at the NBS last year, except that this is a one-dimensional (or perhaps two-dimensional) version. Although our understanding of this phenomenon remains primitive, we believe that the model below shows that the basic physics is in hand.

Recent experiments on optical control of atomic motion have included collimation and focusing of atomic beams, and in some cases, brightness increases as well. Such compression of a beam's phase space volume is possible because of the velocity dependence of the non-conservative optical forces. By focussing all the atoms in such an optically collimated beam to a spot with either a laser[1] or magnetic lens[2] and then recollimating them in the focal region, the beam could be 10^6 or more times brighter than ordinary thermal beams and thereby enable extraordinary sensitivity for new experiments as well as enormous improvements on old ones. Furthermore, this enhancement could be increased by several orders of magnitude if the transverse cooling could cool below the Doppler temperature T_D and if the velocity capture range could be enhanced by two dimensional magneto-optical confinement[3].

2. Experiments. We used diode laser light to actively collimate an atomic beam of ^{85}Rb with transverse one-dimensional optical molasses. The measured angular spread of the beam corresponds to a transverse rms speed of 3 cm/s, well below the $v = \sqrt{(7\hbar\gamma/20M)} \cong$ 10 cm/s corresponding to the Doppler temperature expected for this experimental configuration, including the effects of the dipole radiation pattern. This low velocity, limited only by experimental geometry, is achieved only when a magnetic field of ~20 μT is applied perpendicular to the axis of the circularly polarized light beam.

We use a thermal beam of natural Rb produced by an oven at T ~ 150 ^{o}C with aperture ~ 0.33 mm diam., and a defining aperture of diam. ~ 0.33 mm about 24 cm away (see Fig. 1). The emerging atoms are optically collimated by a pair of counterpropagating laser beams transverse to their motion. The laser light excites the D2 component of the first resonance transition in Rb at λ = 780 nm (natural width = $1/2\pi\tau$ = 6 MHz) in a one dimensional optical molasses. Both the atomic beam and the circularly polarized laser beams are horizontal, and a weak magnetic field (typically vertical) is applied perpendicular to the laser beam axis. The atomic beam profile is measured with a vertically oriented scanning hot tungsten wire, 25 μm in diameter, 1.3 m away from the region of interaction with the laser beam. Since it ionizes virtually every incident Rb atom, its signal is a measure of the vertically integrated beam profile.

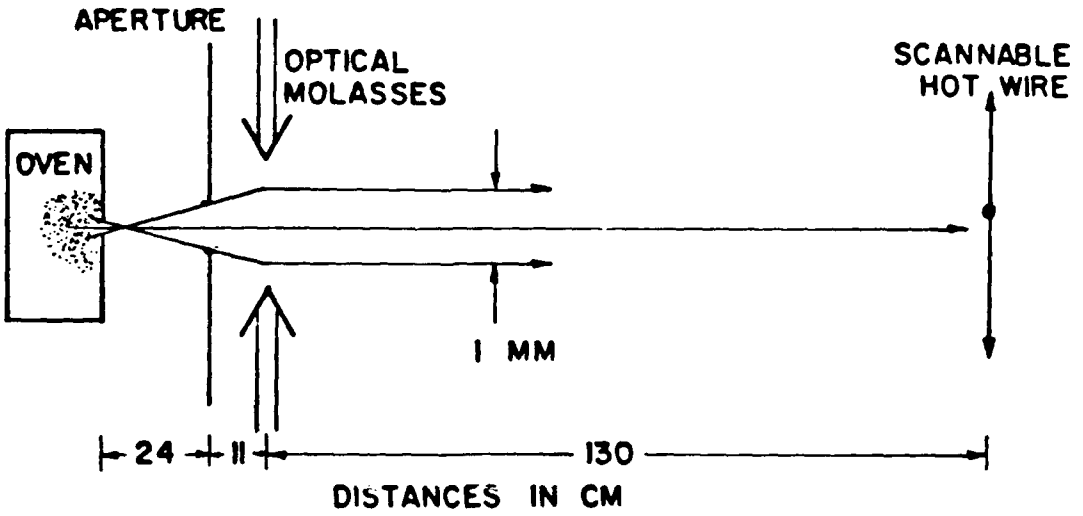

FIGURE 1

The ground state of ^{85}Rb has two hyperfine sublevels whose 3 GHz separation is much larger than the 6 MHz natural width of the transition so that a single laser frequency cannot excite both hfs ground states. Furthermore, the nearly perpendicular atomic and laser beams result in a very small Doppler shift that allows easy resolution of the $(FM_F) = (3,3) \rightarrow (4,4)$ (cycling) transition. Atoms excited to the (4,4) sublevel can only decay to the (3,3) sublevel, so excitation out of the F = 2 hfs sublevel is not needed. Furthermore, the presence of only one laser frequency simplifies the theoretical modelling of the cooling process. The laser frequency is calibrated with a saturated absorption signal from an auxilliary Rb cell at room temperature.

In order to provide both the high power and narrow spectral width needed for optical molasses with diode lasers we use the

technique we have developed for amplifying diode laser light[4]. (A copy of Ref. 4 is in Appendix B.) We exploit the elliptical shape of the diode laser beam, slightly circularized by a pair of anamorphic prisms, to provide a light field extended longitudinally along the atomic beam. We have cut off the Gaussian tails of the laser beam's spatial distribution in both directions, so that the atoms pass through about a $1/e^2$ change in intensity along their flight through the optical molasses. The total power at the interaction region is about 21 mW, apertured to a rectangular shape 8 mm high by 20 mm along the atomic beam.

Collimation of atomic beams by optical molasses is limited by the interaction time and the velocity capture range. In traditional molasses the velocity capture range is $v_c = \gamma/k$ where $k \equiv 2\pi/\lambda$ is the optical wave vector, and the characteristic damping time is $\tau_c \equiv 1/\gamma_c \equiv 2M/\hbar k^2$ for the cycling transition. For Rb, $\tau_c \cong 42\ \mu s$ and $\gamma/k \cong 4.5$ m/s so thermal velocity atoms ($v \sim 350$ m/s) would spend only about $57\mu s \cong 1.4\tau_c$ in a 20 mm long molasses region and could be captured by it if their divergence angles were less than ~13 mrad. Because the damping time τ_c' in this newly discovered process is much smaller, the velocity distribution is much narrower for two reasons: 1) the atoms spend several times τ_c' in the same size interaction region and 2) the temperature limit is much smaller than T_D. The signal is correspondingly smaller because the capture range v_c' is smaller.

3. Results. Figure 2 shows the result of hot wire scans for the circularly polarized collimating laser tuned both above and below atomic resonance. For these scans, the circularly polarized laser beam had average intensity ~13 mW/cm^2 and was tuned ~12.5 MHz above and below atomic resonance. The raw data has been processed before plotting by first subtracting 28% of the raw "no laser" signal from all three traces to correct for the presence of ^{87}Rb in the beam that is not affected by the laser light but is detected by the hot wire. Then 5/12 of the remaining "no laser" signal was subtracted from all three traces because there was no light to pump F=2 atoms into F=3 where they could be collimated.

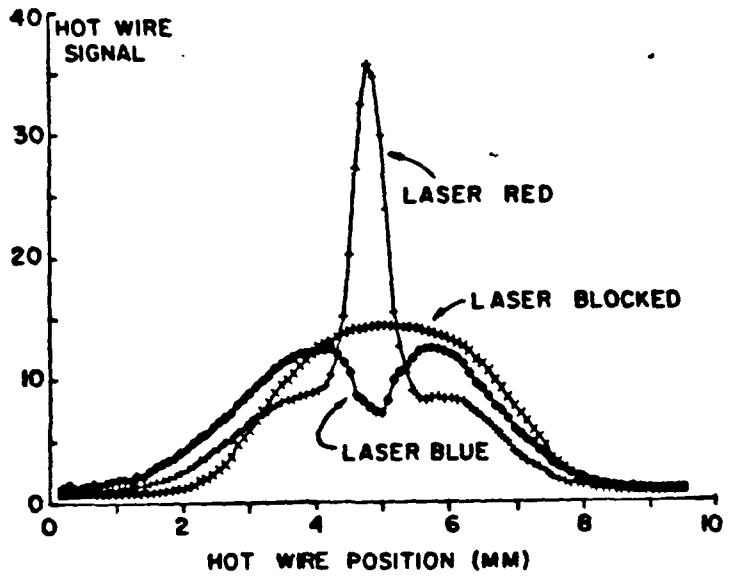

FIGURE 2

To evaluate the collimating effect of the optical molasses we calculate the expected hot wire signal to compare with our measurements. We consider an atomic beam with a cylindrically symmetric trapezoidal spatial distribution whose flat part is 0.33 mm diam.

and whose FWHM is d = 0.48 mm as determined geometrically by the 0.33 mm diam oven and collimating apertures 24 cm apart, and the 11 cm distance from the collimating aperture to the interaction region (Fig. 3). We choose a Gaussian transverse velocity distribution $(1/\alpha\sqrt{\pi})e^{-v^2/\alpha^2}$ and assume that there is no correlation between position and velocity. Certainly there is such a correlation when the atoms enter the molasses, but we assume that the random nature of the absorption and spontaneous emission destroys it if the interaction time is a few times longer than τ_c'.

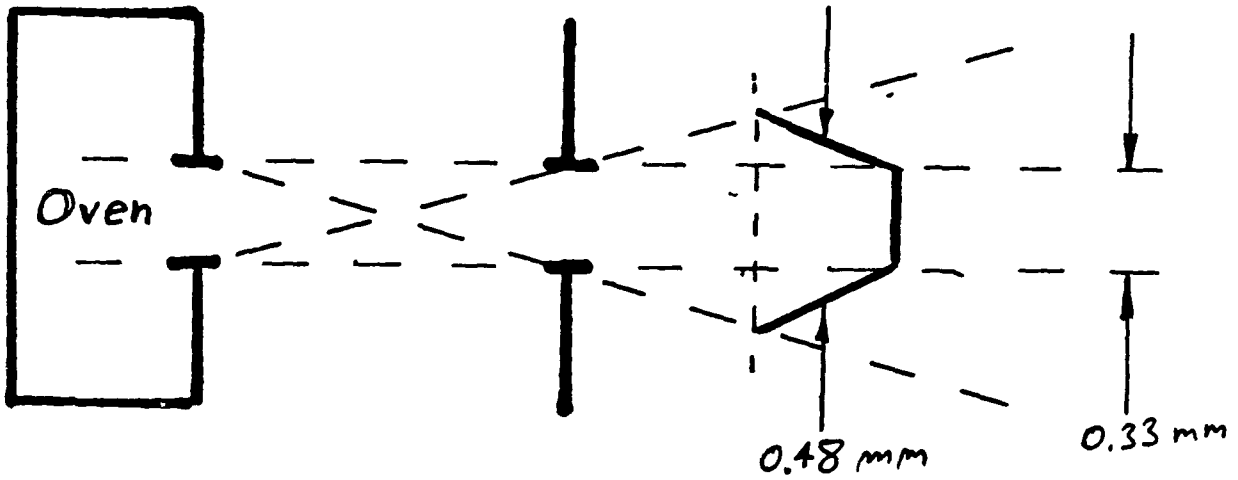

FIGURE 3

We transform this distribution to the plane of the hot wire and integrate over both the vertical direction and over all v's that can contribute to the hot wire signal. The results show that the width of the signal becomes insensitive to α for $\alpha \leq 0.4d/t \sim 4.3$ cm/s, where t is the flight time of the atoms. This corresponds to $v_{rms} = 3.0$ cm/s and a temperature of 10μK. (We note that for a one

dimensional Gaussian velocity distribution $v_{rms} = \alpha/\sqrt{2}$, unlike the three dimensional case where $v_{rms} = \alpha\sqrt{(3/2)}$.)

4. Theoretical Model. In order to model this cooling process, we calculate the force on an atom from the spatial gradient of the Hamiltonian and the atomic density matrix. This automatically allows inclusion of the optical coherences that are known to be important in such problems. However, in the simplified model below, these coherences do not play a role because of our reduction of the problem to a small subset of the atomic energy levels. A solution of the optical Bloch equations for more than two levels is in the works, but it is not in hand at this time. We expect such a solution to differ in detail, but not in any significant way from the model offered below.

The force on an atom is given by $-\langle\nabla H\rangle = -Tr(\rho\nabla H)$ where ρ is the atomic density matrix which we now write in an appropriate coordinate system and a suitably truncated basis. Since the strength of the optical interaction with the atoms is much larger than that of the perpendicular magnetic field, we choose a quantization axis determined by the circular polarization of the light. This light pumps the atoms through all the 2F+1 sublevels toward the (3,3) level of the ground state at rates $\gamma_p(M)$, and then cycles them between (3,3) and the (4,4) level of the excited state. The effect of the field $\vec{B} = B_x\hat{x}$ is simply to mix in other Zeeman sublevels of the ground state at rates given by the Zeeman frequencies $\omega_Z(M)$.

A simple rate equation analysis shows that the competing processes of optical pumping toward the highest M_F levels and Zeeman mixing among these levels results in about 75% of the atoms occupying the two states (3,2) and (3,3). Also, the (4,4) excited state serves only to allow a light shift of the (3,3) state and the (4,3) state serves as an optical pathway from (3,2) to (3,3) and for a (smaller) light shift of (3,2). In our experiment, the optical excitation rate is typically 1/20 of the natural decay rate γ, so that the atomic population is primarily in the ground state. We therefore model this experiment using only the two ground states denoted by (3,2)=|1> and (3,3)=|2>.

In order to solve the Bloch equations $i\hbar\dot{\rho} = [H,\rho] - \hbar\Gamma_\rho$ we write the 2x2 matrices

$$H = \hbar \begin{pmatrix} \tilde{\omega}_1 & \omega_Z \\ \omega_Z & \tilde{\omega}_2 \end{pmatrix} \quad \text{and} \quad \Gamma_\rho = \begin{pmatrix} -\gamma_P\rho_{11} & -\gamma_P\rho_{12}/2 \\ +\gamma_P\rho_{12}/2 & +\gamma_P\rho_{11} \end{pmatrix} \qquad (1)$$

where $\hbar\tilde{\omega}_i = \hbar\delta s/L$ is the energy level shift for the ground state |i> caused by the laser light, and γ_P is the rate of pumping atoms from |1> to |2>. Here s = saturation parameter = $2\Omega^2/\gamma^2$, $\Omega = \Omega(M)$ = Rabi frequency = $\Omega_o(M)\cos(kz)$, δ = detuning = $\omega_{laser} - \omega_{atom}$, and $L = 1 + (2\delta/\Gamma)^2$. From the magnitudes of the Clebsch-Gordon coefficients connecting the appropriate ground and excited states, we find $\gamma_P = 3\gamma s/16(L+s)$ for low light levels. A similar calculation yields $\omega_Z = \sqrt{(3/2)}g_F\mu_B B_x$ where $g_F = 1/3$ is the g factor for the F=3 ground state.

The steady state solutions to the Bloch equations for an atom at rest give

$$\rho_{11}(v=0) = 1 - \rho_{22}(v=0) = \omega_Z^2/(\tilde{\omega}_{12}^2+(\gamma_P/2)^2+2\omega_Z^2), \quad (2a)$$

and

$$\rho_{12}(v=0) = \rho_{21}^*(v=0) = -\rho_{11}(\tilde{\omega}_{12}+ i\gamma_P/2)/\omega_Z \quad (2b)$$

where $\tilde{\omega}_{12} = \tilde{\omega}_1-\tilde{\omega}_2$. We note that in the absence of a magnetic field ($\omega_Z=0$) all the atoms are pumped into $|2\rangle$ ($\rho_{11}=0$) and that a very strong field equalizes the populations of $|1\rangle$ and $|2\rangle$ ($\rho_{11} = \rho_{22} = 1/2$).

For a moving atom, we follow Ref. 5 and calculate the first order velocity dependence of the force with a Taylor expansion. We find

$$\rho'_{11} = \omega_Z^2/(x\tilde{\omega}_{12}^2+2\omega_Z^2+x(\gamma_{P'}/2)^2) \quad (3a)$$

and

$$\rho'_{12} = -\rho'_{11}(\tilde{\omega}_{12}+ i\gamma_{P}'/2)x/\omega_Z \quad (3b)$$

where $\gamma_{P'} = \gamma_P - 4kv\tan(kz)$ and $x = \gamma_P/\gamma_{P'}$. These expressions, together with $\rho_{11}+ \rho_{22} = 1$, are used to calculate the total force on an atom. (Actually ρ'_{12} isn't needed because $\nabla\omega_Z = 0$.) The force contains a velocity independent part that vanishes when averaged over an optical wavelength and is simply the dipole force, and the expected velocity dependent part that survives after such averaging. If this second part is expanded in v using $kv \ll \gamma_P$, the coefficient of the linear term is

$$F = \beta v = v \frac{\hbar k^2 \omega_Z^2 \delta^3 s^2 (1+L)}{12\gamma L(\tilde{\omega}_{12}^2 + (\gamma_P/2)^2 + 2\omega_Z^2)^2} \quad . \qquad (4)$$

Since an increase in light intensity without a concomitant increase in magnetic field would inhibit the mixing caused by the field, it is not suprising to see that the intensity appears in the denominator of Eq. 4 in the high intensity limit. If the field were linearly scaled with light intensity (Ω^2), we find the damping constant independent of intensity as expected. From Eq. 4 we can calculate that the damping time $\tau_c' << \tau_c$ and this is supported by our measurements showing that over a large range of parameters, shortening the length of the interaction region by 25% has little effect on the measured width of the distribution.

Figure 4a shows the measured width of one-dimensional collimated atomic beam vs applied magnetic field for two different laser detunings. This data was all taken with s = 10, but we also have data for s = 3 and 1. We can also calculate the heating rate of the atoms that derives from the randomness of the spontaneous emission, and then combine this with Eq. 4 to get a temperature. Figure 4b shows how this calculated temperature varies with field for various detunings, again at s = 10.

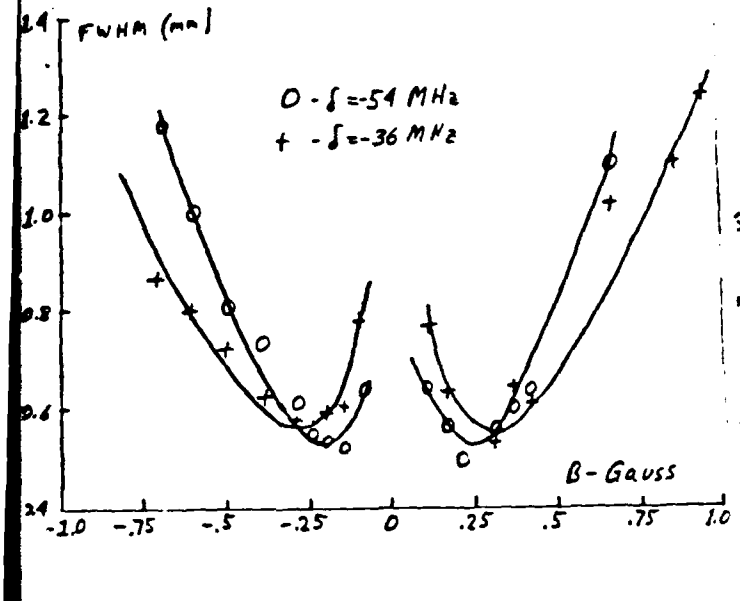

FIGURE 4a

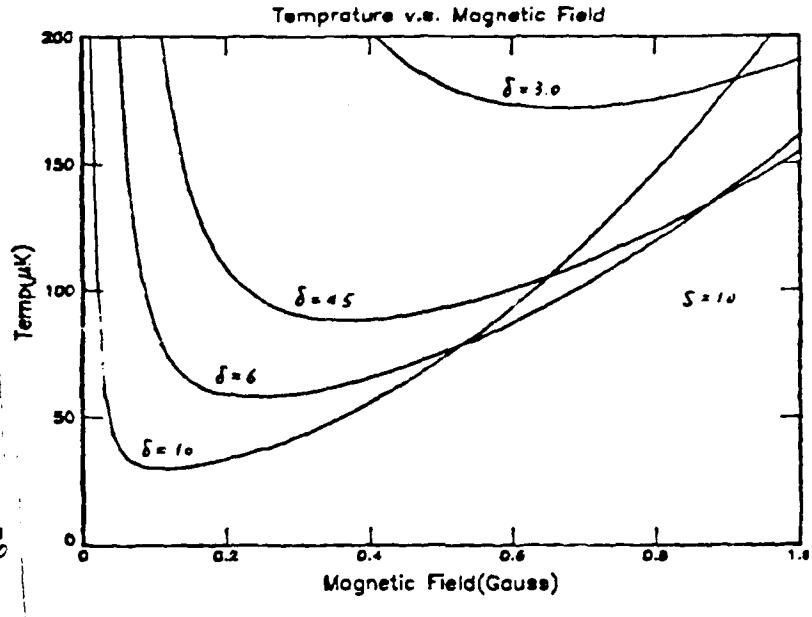

FIGURE 4b

From several sets of data of the type shown in Fig. 4a we can extract the optimum value of field for each detuning, again at s = 10, and these are plotted in Fig. 5. The solid curve is calculated from Eq. 4. A paper describing the discovery of this new cooling mechanism is in preparation for Physical Review Letters.

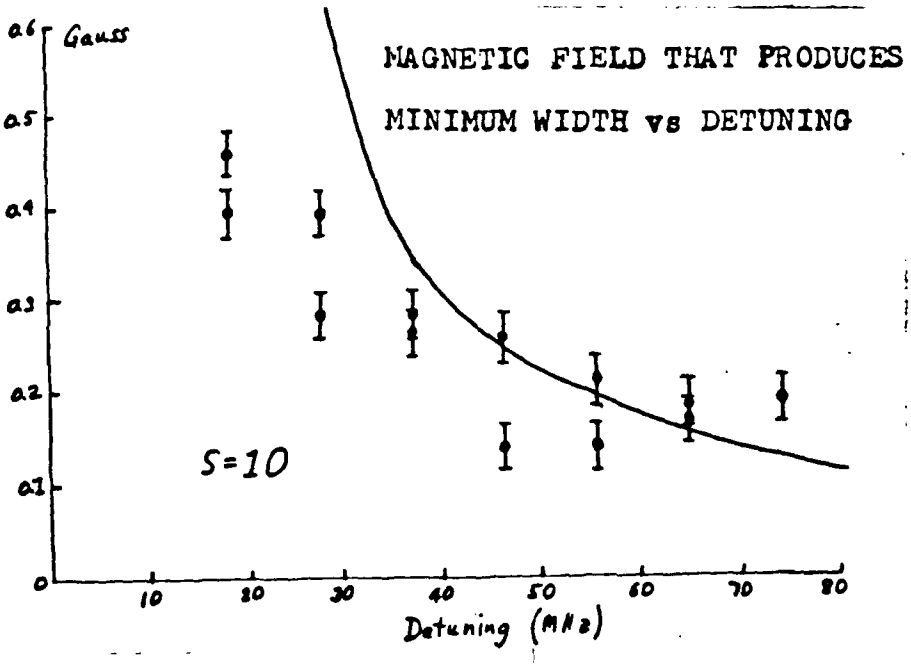

FIGURE 5

B. Imaging Atomic Beams

We have also performed optical collimation experiments in two dimensions to make a very intense beam of atoms. Measuring a beam profile in two dimensions would require two hot wires scanning in perpendicular directions, and any asymmetry in the line shape could produce ambiguity. It is therefore very desirable to have a neutral atom imaging device.

We have devised a new method for observing the spatial distribution of atoms in the beam. A plane Ni mesh is mounted perpendicular to the atomic beam and is heated to several hundred ^{o}C to operate as a surface ionization detector much like a hot wire (see Fig. 6). Ions emitted from the hot grid in the upstream direction are driven back through its holes by the electric field produced by a voltage between it and a second (repeller) grid mounted upstream from it. Once downstream of the hot grid, ions are accelerated into a pair of multichannel plate (MCPs) electron multipliers whose output goes to a phosphor coated screen which is viewed by a standard TV camera. The camera's output is fed to a frame grabber in a computer where the image can be analyzed. The ~500 μm resolution of this system, corresponding to $v \approx 13cm/s$, is limited by the spatial spread of the charged particles in flight between the hot grid and the MCPs, and between the MCPs and the phosphor.

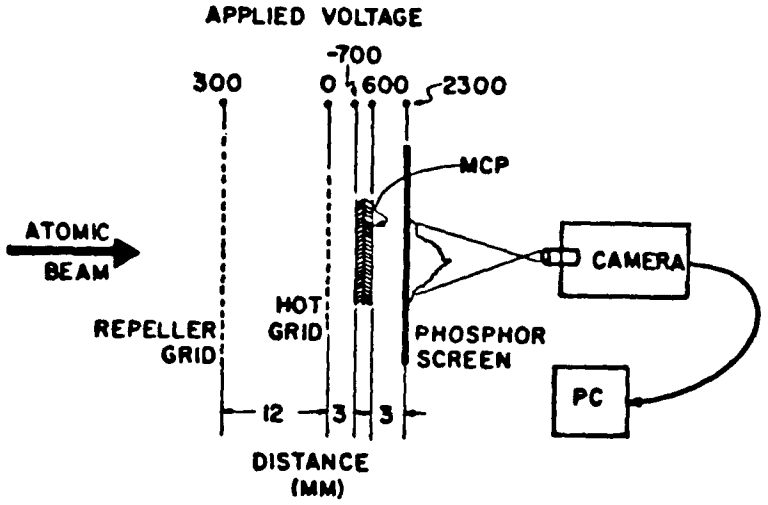

FIGURE 6

Figure 7 shows the image formed by the neutral atom camera of two-dimensional molasses acting on atomic beam. The outline of the circular beam spot represents a 6 mm diameter image on the phosphor ($1/30^{th}$ sec, no image averaging). The 7 mW molasses laser beams were nearly uniformly intense and rectangular, about 8 x 20 mm. The detuning was about -30 MHz for A and about +30 MHz for B. Note the collimation for the red detuning and the divergence for the blue detuning. A paper describing this neutral atom imaging system will be submitted to Review of Scientific Instruments.

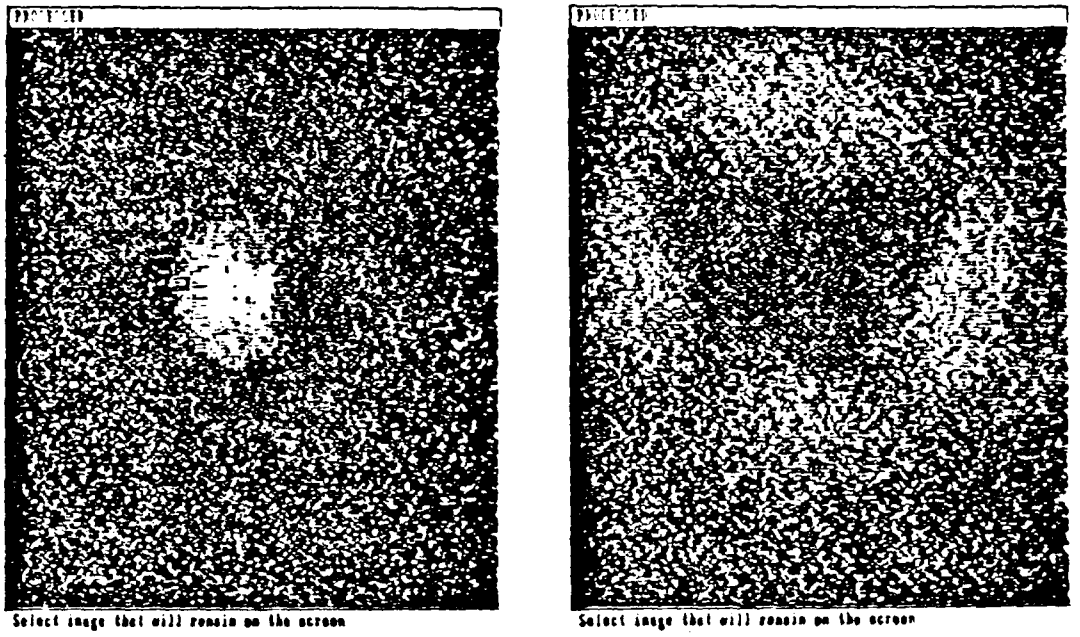

FIGURE 7

C. Diode Laser Experiments at Stony Brook

1. Diode Laser Technology. Diode laser experiments require a certain amount of technological expertise, and we have been working to develop that. Our work with diode lasers and their application to controlling the motion of atoms has made considerable progress, and our paper describing the amplification of diode laser light has been published in Applied Optics. It is reproduced in Appendix B.

2. Diode Laser Aging. Part of the diode laser lore concerns their aging. We have found that lasers may drift off the resonance frequency during a few hundred hours of usage, and we suspect that they may age with running time. This idea is supported by other workers. We might therefore expect that another few hundred hours of use would cause them to drift back on resonance in another mode.

We have constructed an "aging facility" consisting of multiple mounts on which we can run these for a week or two, and then try them again. The hope is that a resurrection scheme can be developed to enable us to use the several perfectly working, off-resonance diodes we have accumulated. This project will be done by undergraduates during the summer of 1989.

D. High Vacuum System for Trap and Molasses

The high vacuum system planned from the outset of these experiments at Stony Brook is essentially complete. We have obtained coated windows for its ports and built a large reentrant windowed port for easy optical access to the central region of the chamber. The atomic beam source, complete with steerable oven, is mounted and pumped down. It is separated from the main chamber by a small aperture to assist in differential pumping so that it won't corrupt the high vacuum region. At present the new atomic beam system is ready for use, but has not been used yet because our attention has been focussed on the new discovery discussed above.

E. Magnetic Trapping of Neutral Atoms

The theoretical problem of the translational quantum states of a spin 1/2 atom in a magnetic trap has been described in some detail in our paper sent to the special issue of the J. Opt. Soc. Am. There we have presented a discussion of the shifts and widths of the levels that derive from the coupling between the quasi-discrete

states and the continuum. Since the quantization problem is better defined for magnetostatic traps than for optical or magneto-optic traps, the original quadrupole (two-coil) trap was the subject of this paper.

The calculations show that attaining the low temperatures necessary to see some of these effects is a major task, but not outside the limits of laser cooling as we know it today. We therefore conclude that this calculation may have an important impact on future experiments. Attainment of this energy regime would overcome the spectroscopic broadening effects due to motion of an atom in a non-uniform magnetic field and might lead also to Bose-Einstein condensation.

F. Trapping Metastable Helium

1. Introduction. Since the earliest experiments on optical pumping of helium there has been interest in generating light to excite the first resonance transition from the metastable 2^3S_1 state to the $2^3P_{0,1,2}$ states (lifetime $\tau \sim 95$ nsec). For 25 years these experiments were done with light from resonance lamps, but the advent of LNA in 1985 provided the opportunity for laser excitation of this important transition.

Recently developed LNA lasers were intended for optical pumping of gaseous helium and therefore operated multimode with spectral width large enough to span the the Dopper profile at room

temperature (more than 1 GHz). Our intention is for use with an atomic beam or for laser cooling, both of which require much narrower spectral width, and our laser is correspondingly designed to facilitate single mode operation. The cavity is therefore made as short as practical to separate the longitudinal modes, and the pumping volume is chosen to favor a single cavity spatial mode.

Nd:YAG lasers operate at λ = 1.064 μm, about 6000 GHz and many linewidths away from the He resonance line. LNA is another host lattice for Nd^{+3} ($La_{1-x}Nd_xMgAl_{11}O_{19}$) that splits and shifts the laser spectrum relative to Nd:YAG. There are two principle laser bands, the stronger one at λ = 1.053 μm and the weaker (but desirable one) at λ = 1.083 μm. Earlier workers have discriminated against the stronger one with a birefringent (Lyot) filter, but we have chosen to use a dichroic coating on the end of the crystal to do this job. The result is a much more compact laser cavity with fewer components to align.

2. Our Design. The absorption spectrum of Nd^{+3} ions in LNA has a strong peak at λ = 794 nm, convenient for pumping with diode lasers and therefore more efficient than excitation with ion lasers. We operate a 500 mW Spectra Diode Labs 2430C diode laser array at λ = 794 nm (our earlier LNA laser had worked quite well with a 200 mW 2420C device). Its output is collimated, circularized by a pair of anamorphic prisms, and focussed by a 6.5 mm working distance lens to a ~100 μm spot just inside the dichroic coated end of the crystal (see Fig. 8). This highly specialized coating transmits

more than 90% of the pump light, reflects 99% of the 1.083 mm light, yet reflects only 80% of the unwanted component at 1.053 μm so that the laser operates on the desired band (see Fig 9). The other end of the 10 mm long crystal is anti-reflection coated at 1.083 μm.

PLANE – PARALLEL CAVITY

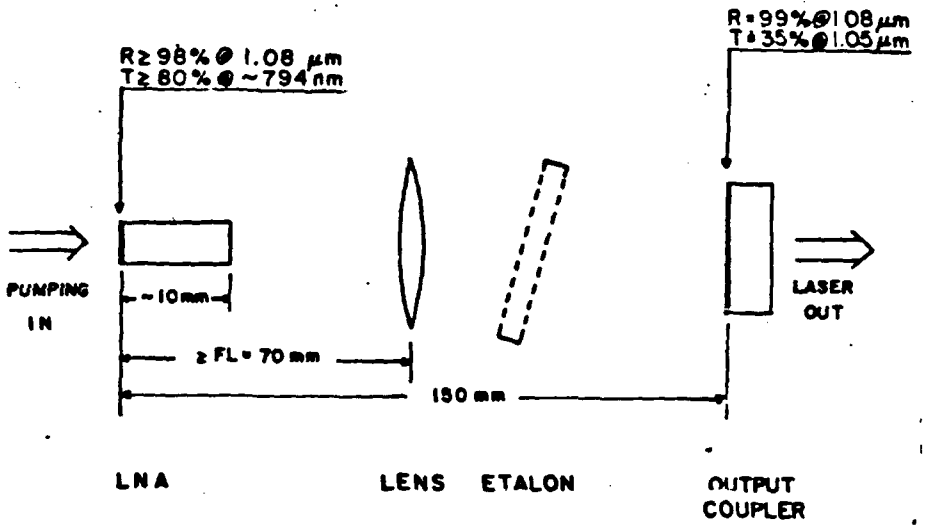

FIGURE 8

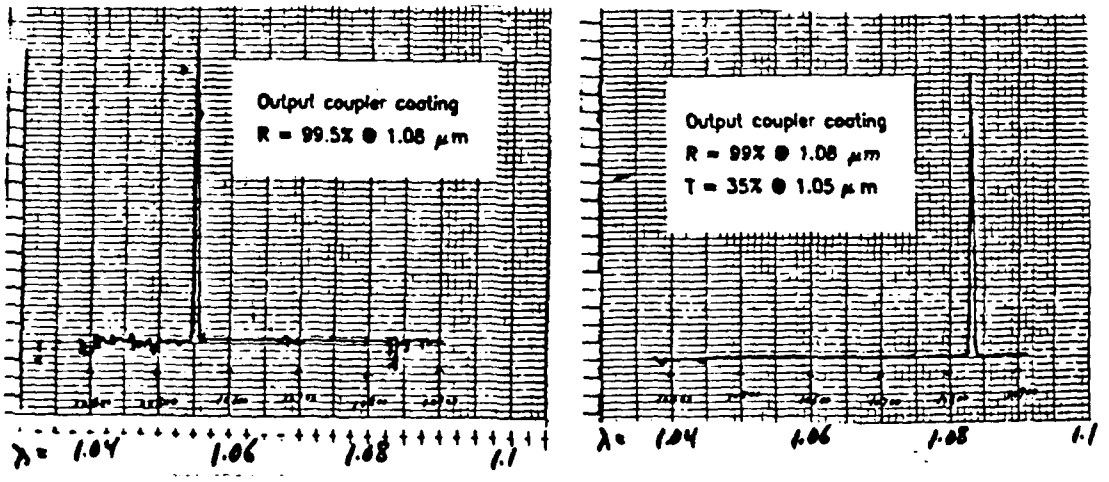

FIGURE 9

The light from this pumped region is collimated by an anti-reflection coated lens and reflected by a plane output mirror that transmits a few percent at λ = 1.083 nm. In our preliminary experiments we have tried mirrors of various transmissions and even some with the same dichroic coating as applied to the crystal. In order to select a single mode of the cavity, we have placed a low finesse, solid quartz etalon between the lens and the output mirror. The etalon is 1/4 mm thick with reflection coefficient R = 60% on each surface, thus having FSR of 400 GHz (15 A), finesse of $\pi\sqrt{R}/(1-R) = 6$, and resolution ~ 67 GHz. Since the laser cavity has a mode separation of about 1 GHz, the etalon has about 65 cavity modes between its 50% points. With a little care, we can make it select a single one of them sufficiently well. We have operated the laser in a single transverse mode and tuned it to the He resonance frequency.

3. Results and Performance of Laser. The efficiency of operation of the laser depends on the absorption of both pump and laser light, reflectivity of the coatings, and matching the pumped volume of atoms to the laser cavity mode. For those quantities relevant to the LNA crystal only, we can calculate a "figure of merit" given by $FM = (1-r_d)(1-e^{-L/x})(R_d)(e^{-L/X})(1-R_a)$ where r,R are reflection coefficients, x,X are absorption lengths, (lower case x and r refer to λ = 794 nm and upper case X and R refer to λ = 1.08 μm), L is the length of the crystal, d refers to the dichroic coated end of the crystal, and a refers to the anti-reflection coated end (at 1.08 μm). Because more than 95% of the diode laser light is

absorbed, we are not concerned with the properties of the anti-reflection coating at 794 nm (r_a). We expect that FM provides a measure of the crystal's performance. We have been measured these quantities for our several LNA samples (obtained from Airtron Corp. and Union Carbide Corp.) with and without coatings for the purpose of making the best laser. Some of these measurements must be carefully corrected for reflection losses, which we also measure by tilting the crystal just a few degrees.

These crystals have all been tested in the laser. We measure the threshold and differential efficiency by varying the pump laser light power. Figure 10 shows a typical laser efficiency curve and Fig. 11 shows both efficiency (circles) and threshold (triangles) vs. FM for some of our crystals.

Because the measured value of FM for one crystal whose performance was very poor was not exceptionally low, we set out to determine why it behaved so badly. We began by X-ray analysis of several crystals, and this showed that they were all cut within a few degrees of the crystal axis, but that the "bad" one was probably cut with the cylinder axis along the crystal a-axis instead of the more laser efficient c-axis. This was later confirmed by polarization analysis, thus explaining its poor performance.

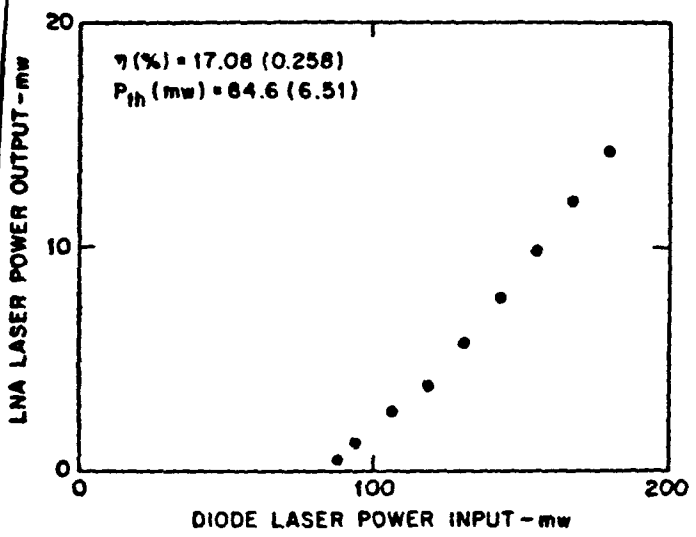

FIGURE 10

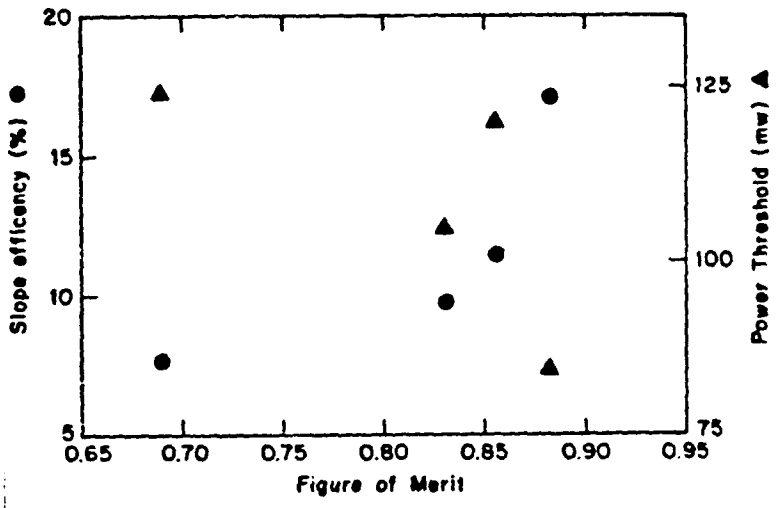

FIGURE 11

The lowest order spatial mode of our laser cavity has a spot size of about 100μm, and the diode laser beam spot is focussed to about the same size so the pumped volume of atoms is well matched to the cavity. More than 95% of the output power is in a single longitudinal mode, measured by observing the envelope of the rf output from the scanning Michaelson interferometer in our wavemeter, and the transverse mode is almost pure TEM_{00}.

We have tuned the laser to the resonance frequency of helium, measured by observing the absorption of light in a sealed cell with a weak rf discharge running. Once tuned to the resonant frequency, the laser can be turned off and left for days, and when it is restarted it is still on resonance to within the Doppler width (~1 GHz). To test its stability, and alo its ultimate necessary performance capabilities, we have performed saturated absorption

spectroscopy on the same cell. The signals (with a lockin) are strong; a sample spectrum of the D1 and D2 lines is shown in Fig. 12. The width is about 5 MHz, determined primarily by collision broadening in the gas whose pressure is 0.2 Torr. A paper describing the development of this laser is in in preparation for Applied Optics.

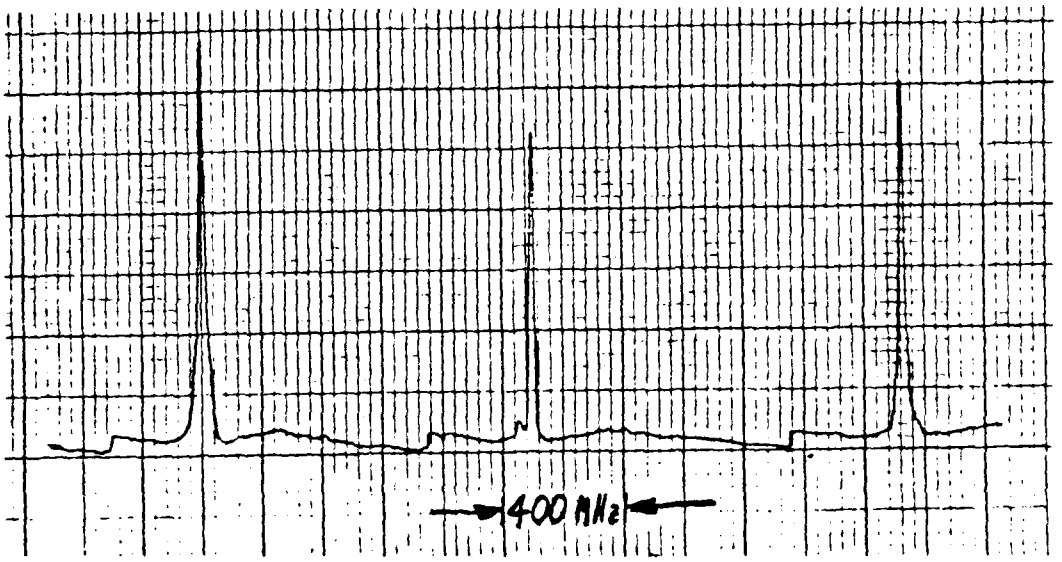

FIGURE 12

G. Experiments at NIST

The PI continues to collaborate with the group led by Bill Phillips at NIST (also supported by the ONR). The past year has been one of consolidation and study of the discoveries of the previous year. A very large paper (~100 pages) was prepared for the special issue of the J. Opt. Soc. Am. mentioned above, and this consumed most of the group's effort during the spring of 1989.